Electrogenerated Chemiluminescence by in Situ Production of Coreactant Hydrogen Peroxide in Carbonate Aqueous Solution at a Boron-Doped Diamond Electrode

Electrogenerated Chemiluminescence by in Situ Production of Coreactant Hydrogen Peroxide in Carbonate Aqueous Solution at a Boron-Doped Diamond Electrode

Irkham,[1] Andrea Fiorani,[1] Giovanni Valenti,[2] Naoki Kamoshida,[1] Francesco Paolucci,[2] Yasuaki Einaga*[1,3]

[1] Department of Chemistry, Keio University, 3−14−1 Hiyoshi, Yokohama 223−8522, Japan

[2] Department of Chemistry "G. Ciamician", University of Bologna, Via Selmi, 2, 40126 Bologna, Italy

[3] JST-ACCEL, 3−14−1 Hiyoshi, Yokohama 223−8522, Japan

E-mail: einaga@chem.keio.ac.jp

KEYWORDS Electrogenerated chemiluminescence, Carbonate, Peroxydicarbonate, Hydrogen peroxide, Boron-doped diamond

ABSTRACT: An electrogenerated chemiluminescence (ECL) system by the in-situ coreactant production, where $Ru(bpy)_3^{2+}$ emission is generated at a boron-doped diamond (BDD) electrode, is presented. The system takes advantage of the unique properties of BDD to promote oxidation of carbonate (CO_3^{2-}) into peroxydicarbonate ($C_2O_6^{2-}$), which further reacts with water to form hydrogen peroxide (H_2O_2), which acts as a coreactant for $Ru(bpy)_3^{2+}$ ECL. Investigation of the mechanism reveals that ECL emission is triggered by the reduction of H_2O_2 to hydroxyl radicals ($OH^\bullet$) which later react with the reduced $Ru(bpy)_3^{+}$ molecules to form excited states, followed by light emission. The ECL signal was found to increase with the concentration of CO_3^{2-}, therefore with the concentration of electrogenerated H_2O_2, although at the same time, higher concentrations of H_2O_2 can quench the ECL emission resulting in a decrease in intensity. The carbonate concentration, pH and oxidation parameters, such as potential and time, were optimized to find the best emission conditions.

INTRODUCTION

Sensors and biosensors take enormous advantage of electrochemical methods,[1,2] of which electrogenerated chemiluminescence (ECL) is a leading transduction technique, which is used in clinical diagnostics,[3] and is prominent in point-of-care testing.[4]

Thanks to the combination of electrochemical stimulus and luminescent response, ECL showed *(i)* the best signal to noise ratio, theoretically without any background emission, with a detection limit typically in the range of pM; *(ii)* broad dynamic range of more than six order of magnitude, *(iii)* rapid measurement (i.e., few seconds), and *(iv)* small working volume for analysis (tenth of a µl).

In ECL process the signal generation is achieved by homogeneous electron transfer between the radical species generated at the electrode, to form a light emitting excited species.[5–8] The so-called coreactant method is mainly applied for analytical purposes, where tris(bipyridine)ruthenium(II) $Ru(bpy)_3^{2+}$ and tri-*n*-propylamine is the leading couple, as the luminophore and coreactant, respectively. The overall ECL mechanism leads to consumption of the coreactant, a sacrificial molecule, with continuous regeneration of the luminophore, in a catalytic cycle. The mechanisms of coreactant ECL can be achieved for oxidation or reduction reactions, for example tri-*n*-propylamine (oxidative-reduction)[9] and peroxydisulfate (reductive-oxidation),[10] respectively.

The advantage of coreactant ECL, compared to annihilation ECL, where both the cation and the anion of the luminophore are needed, is the feasibility of mechanisms that work in aqueous solutions, within the water potential window. Although coreactant approach paved the way for extended analytical applications in commercial immunoassay and biosensors in biocompatible environments, the high concentration of coreactants shows some disadvantages such as toxicity and may represent a severe drawback in some bioanalytical applications.[11,12] In addition the electrochemical reactions that trigger ECL occurs typically at quite high electrodic potential and could be affected by the electrode material and its surface proprieties.[13] Therefore the analytical signal measured (i.e., light) may differ significantly depending on the type of electrode used. For example, applying anodic currents at an electrode in an aqueous solution leads to surface modifications, such as the formation of metal oxides[14] and surface oxygen terminations.[15] On the other hand, cathodic currents may drive sufficient hydrogen evolution to hamper ECL by overwhelming the electrochemical reactions of the luminophore and coreactant. Nevertheless, reductive-oxidation ECL has been reported on nanoporous gold electrodes,[16] carbon paste electrodes[17] and glassy carbon electrodes,[18] however, this

mechanism is still less common than the oxidative-reduction mechanism.

Recently, we demonstrated that boron-doped diamond (BDD) is a superior electrode material for reductive-oxidation.[19] Furthermore, we reported a new ECL system, the $Ru(bpy)_3^{2+}/S_2O_8^{2-}$ system, achieved only at BDD electrode, where peroxydisulfate for the ECL reaction is electrogenerated by oxidation of the unreactive sulfate precursor.[20] Since the oxidation of sulfate occurs at high overpotential (E^0 = 2.01 V vs SHE,[21] 2.52-3.08 V vs NHE[22]), the generation of ECL is possible only thanks to the wide potential window of BDD, combined with the electro-oxidation of SO_4^{2-}.[23] Other reactive compounds are also known to be generated using BDD electrodes, such as hydrogen peroxide from hydroxyl oxidation[24–26] (E^0 = 1.77-1.91 V vs SHE),[27–29] which is also a coreactant for ECL.[18,30,31] Although BDD is able to electrogenerate hydrogen peroxide by oxygen reduction, efficient production requires an acidic pH[23,25,26,32] that might enhance the hydrogen evolution process at cathodic currents, and consequently affect the ECL reductive-oxidation mechanism.

On the other hand, hydrogen peroxide can be conveniently prepared by electro-oxidation of carbonate in aqueous solution (E^0 $CO_3^{2-/\bullet-}$ = 1.59 V at pH 12 vs NHE)[33–35] at a BDD electrode.[36–39] The electrogeneration mechanism includes the formation of peroxydicarbonate ($C_2O_6^{2-}$), mediated by $OH^\bullet$, which reacts with water to form hydrogen peroxide and carbonate (CO_3^{2-}).

Here, we report on a coreactant free $Ru(bpy)_3^{2+}/CO_3^{2-}$ ECL system that proceeds by the in-situ production of hydrogen peroxide at BDD electrode via carbonate oxidation and subsequent peroxydicarbonate hydrolysis, giving the overall ECL reaction depicted in Figure 1.

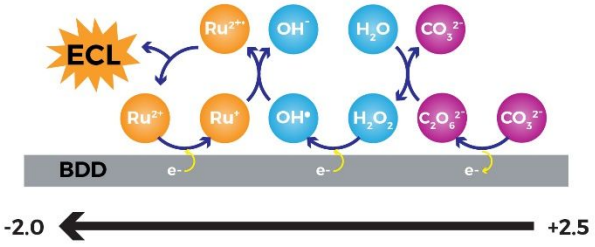

Figure 1. ECL scheme of the proposed reaction mechanism for the $Ru(bpy)_3^{2+}/CO_3^{2-}$ system at a BDD electrode. The colors describe the electrochemical reactions on carbonate (pink), the H_2O_2 coreactant (blue), and the ruthenium luminophore (orange). Ru = $Ru(bpy)_3$.

EXPERIMENTAL

Materials. All the reagents were obtained commercially and used without further purification. $Ru(bpy)_6Cl_2 \cdot 6H_2O$ was purchased from TCI (Japan), $HClO_4$, $NaClO_4$, Na_2CO_3, H_2O_2 from WAKO (Japan), and $Na_2CO_3 \cdot 1.5H_2O_2$ from Sigma-Aldrich. D_2O (99.9%) was obtained from Cambridge Isotope Laboratories, Inc. Acetone (TCI) and trimethoxyborane (TCI) were used in the preparation of the BDD. Double distilled water (18.2 MΩ at 25°C) was obtained from a Simply-Lab water system (DIRECT-Q3 UV, Millipore).

Preparation of the BDD Electrodes. BDD films were deposited on silicon (111) wafers (Shinwa Tsusho) using a microwave plasma-assisted chemical vapour deposition (MPCVD) system (CORNES Technologies/ASTeX-5400). Acetone and trimethoxyborane were used as the carbon and boron sources, respectively, with an atomic ratio of B/C ≈ 1% ([B] in BDD ≈ 2×10^{21}/cm^3). The surface morphology of the BDD was examined with a field emission scanning electron microscope (SEM, JEOL JCM-6000). Raman spectra were recorded with an Acton SP2500 (Princeton Instruments) with excitation wavelength of 532 nm from a green laser diode at ambient temperature (Figure S1).

Electrochemical Measurements and ECL. All electrochemical measurements were conducted with a potentiostat (PGSTAT302N, Metrohm) using a single-compartment three-electrode Teflon cell with 1% BDD, Pt or glassy carbon (GC) as the working electrode, a Pt spiral as the counter electrode and an Ag/AgCl (saturated KCl) electrode as the reference electrode. The working electrode area was 0.635 cm^2. The ECL signal was measured with a photomultiplier tube (PMT, Hamamatsu R928) placed at a fixed height from the electrochemical cell, inside a dark box. A high voltage power supply socket assembly with a transimpedance amplifier (Hamamatsu C6271) was used to supply 500 V to the PMT, using an external trigger connection to the potentiostat DAC module. Light/current/voltage curves were recorded by collecting the amplified PMT output signal with the ADC module of the potentiostat. ECL spectra were collected by a SEC2000 Spectra system UV-visible spectrophotometer (ALS Co., JP).

Prior to each measurement, the BDD surface was pretreated to guarantee reproducibility, with cathodic reduction at −3.5 V followed by anodic oxidation at +3.5 V (total fixed charge of 0.1 C in each step) in 0.1 M $NaClO_4$ solution. The GC (Tokai Carbon, Japan) and Pt (Nilaco Co., Japan) electrodes were cleaned with a 0.5 µm alumina suspension on cloth tape, then sonicated in double distilled water for 5 min (2 times), and dried with a nitrogen stream. All experiments were carried out at room temperature.

In Situ Attenuated Total Reflectance-Infrared (ATR-IR) Measurements. The BDD film used for the in-situ IR measurements was deposited onto a Si ATR prism using the MPCVD system, as described above. The carbon and boron sources were methane and trimethylboron, respectively, with a B/C ratio of 1%. The BDD on the prism, a glassy carbon rod, and Ag/AgCl (saturated KCl) were used as the working, counter, and reference electrodes, respectively, and controlled by a PGSTAT204 (Metrohm). Spectra were recorded with a Fourier-transform IR spectrometer (FT/IR-6600, JASCO Corp.) with a liquid-nitrogen-cooled mercury-cadmium-telluride (MCT) detector. Each spectrum was measured at a resolution of 4 cm^{-1}.

To record the infrared spectra (ATR-IR), the following 4-step sequence was carried out: 1) background (BG) acquisition at one potential (E_{base}); 2) application of an oxidation pulse at 2.5 V for 20 seconds (t_{Ox}); 3) acquisition of a second spectra at E_{base} and subtraction of the BG spectrum; 4) application of 0 V while bubbling nitrogen for 10 seconds to restore the initial conditions (Figure S2). This sequence was repeated 25 times, with 20 spectra acquired in step 3, so that each spectrum was the average of 500 scans.

Subtractively normalized interfacial Fourier-transform infrared spectroscopy (SNIFTIRS) mode was also employed with same spectroelectrochemical setup. The detailed procedure for this is given in the Supporting Information (Figure S2).

RESULTS AND DISCUSSION

The electrochemical and the ECL properties of $Ru(bpy)_3^{2+}$ in Na_2CO_3 aqueous solution at a BDD electrode were first investigated by cyclic voltammetry (CV). The CV was conducted by first scanning the potential from 0 V to 2.5 V followed by scanning to a negative potential up to −2.5 V. Figure 2a (red line) shows that a high ECL signal was observed during the CV starting from −1.5 V reaching a peak at around −1.9 V. This ECL emission is due to a combination of the unique properties of BDD, which combine an efficient generation of peroxydicarbonate, and a high overpotential for the hydrogen evolution reaction, allowing ECL to be obtained through reductive-oxidation mechanism. ECL emission was observed only with the carbonate solution, while no significant signal was observed with the $NaClO_4$ solution (Figure 2a, black) (see discussion for further details about the background signal). The same experiment conducted with conventional electrode materials such as GC and platinum could not generate any ECL signal (Figure S3), although carbonate can be oxidized at Pt electrodes,[40] and GC electrodes (Figure S3, inset), the higher current for the hydrogen evolution reaction prevents the generation of ECL

The first positive scan generated the peroxydicarbonate from the oxidation of carbonate, which further reacts with water to produce hydrogen peroxide according to the following mechanism:[40,41]

$$CO_3^{2-} \rightarrow CO_3^{\bullet-} + e^- \quad (1)$$

$$2CO_3^{\bullet-} \rightarrow C_2O_6^{2-} \quad (2)$$

$$C_2O_6^{2-} + 2H_2O \rightarrow H_2O_2 + 2HCO_3^- \quad (3)$$

Peroxydicarbonate hydrolysis was confirmed with a rotating ring-disk electrode where the current for H_2O_2 oxidation was simultaneously measured during oxidation of the carbonate.[40] At a BDD electrode, the oxidation of the carbonate is mediated by $OH^\bullet$ generated from hydroxide oxidation:[24,42]

$$BDD + OH^- \rightarrow BDD(OH^\bullet) + e^- \quad (4)$$

Therefore, we can write the overall equation for the oxidation of the carbonate as:[37-39,43]

$$2BDD(OH^\bullet) + 2CO_3^{2-} \rightarrow 2BDD + C_2O_6^{2-} + 2OH^- \quad (5)$$

where BDD represents the active site on the electrode surface.

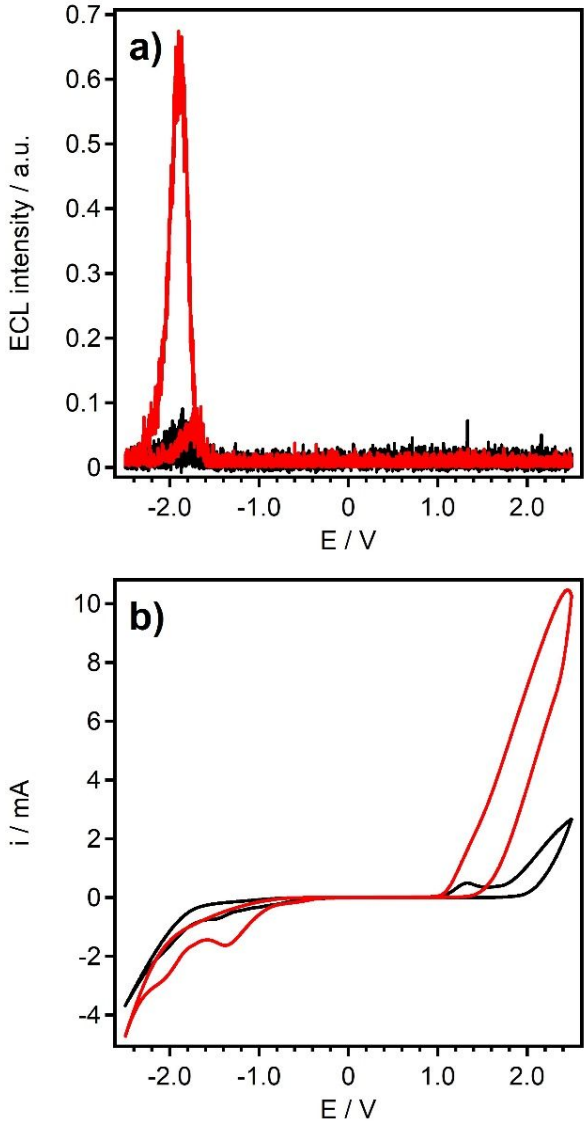

Figure 2. Comparison between (a) the ECL measurements and (b) the CVs of 10 µM $Ru(bpy)_3Cl_2$ in aqueous solutions (pH 11.5) of 100 mM Na_2CO_3 (red) and 100 mM $NaClO_4$ (black). The potential was swept from 0 V, first to 2.5 V then to −2.5 V. Scan rate: 100 mV/s.

The CV in Na_2CO_3 (Figure 2b, red line) shows a significantly higher anodic current compared to that in $NaClO_4$ (Figure 2b, black line), confirming the oxidation process of the carbonate. For both electrolytes, an onset oxidation potential of 1.1 V was observed, with a peak at 1.3 V in $NaClO_4$ solution. This was previously reported to be the oxidation of hydroxide ions at a BDD electrode (eq. 4),[44,45] which mediates the oxidation of CO_3^{2-} (eq. 5). The second scan, toward negative potentials, generated the ECL with the H_2O_2 produced from the EC oxidation mechanism of the carbonate, with the following likely mechanism, as proposed by Choi and Bard for the $Ru(bpy)_3^{2+}/H_2O_2$ system:[18]

$$H_2O_2 + e^- \rightarrow OH^\bullet + OH^- \quad (6)$$

$$Ru(bpy)_3^{2+} + e^- \rightarrow Ru(bpy)_3^{+} \quad (7)$$

$$Ru(bpy)_3^{+} + OH^\bullet \rightarrow Ru(bpy)_3^{2+*} + OH^- \quad (8)$$

$$Ru(bpy)_3^{2+*} \rightarrow Ru(bpy)_3^{2+} + h\nu \quad (9)$$

The ECL emission is obtained after both H_2O_2 (eq 6) and $Ru(bpy)_3^{2+}$ (eq 7, E^0 = −1.48 V vs Ag/AgCl) are reduced, followed by homogeneous electron transfer (eq 8), which leads to the emission of light (eq 9). In the cathodic scan, the reduction peaks at ≈ −0.8 V are from sp^2-carbon impurities on the BDD surface. The second peak at ≈ −1.5 V for the $NaClO_4$ solution is oxygen reduction,[43,46,47] since it can be easily removed after nitrogen bubbling (Figure S4). The cathodic scan for Na_2CO_3 shows a peak starting at ≈ −1.5 V, at the same potential as ECL, likely to be oxygen and peroxydicarbonate reduction, since the hydrogen peroxide reduction peak is not clearly observed even when using H_2O_2 directly (Figure S5). The ECL spectrum confirms the emission from $Ru(bpy)_3^{2+*}$ (Figure S6), with a peak emission wavelength at ≈ 620 nm. Without $Ru(bpy)_3^{2+}$, no ECL signal was obtained (Figure S7). Furthermore, the ECL emission was triggered by hydrogen peroxide produced in the first positive scan, via the EC mechanism of electrogenerated peroxydicarbonate, and not from hydroxyl radicals produced by hydroxide oxidation[48] (eq 4) or H_2O_2 from the recombination of hydroxyl radicals,[25] because only slightly detectable ECL signal was observed in the $NaClO_4$ solution (Figure 2a, black line).

In line with this hypothesis, no ECL was observed when the first positive scan was swept to a value insufficient to generate peroxydicarbonate (Figure S8), although in this case, a weak ECL signal could be observed. This signal is likely to have originated from the annihilation reaction mechanism between oxidized $Ru(bpy)^{2+}$, electrogenerated at E^0 = 1.07 V (vs Ag/AgCl), and the reduced $Ru(bpy)^{2+}$, as follows[49]:

$$Ru(bpy)_3^{3+} + Ru(bpy)_3^{+} \rightarrow Ru(bpy)_3^{2+*} + Ru(bpy)_3^{2+} \qquad (10)$$

Moreover, the background emission in the $NaClO_4$ solution (Figure 2a, black line) can be ascribed to this mechanism.

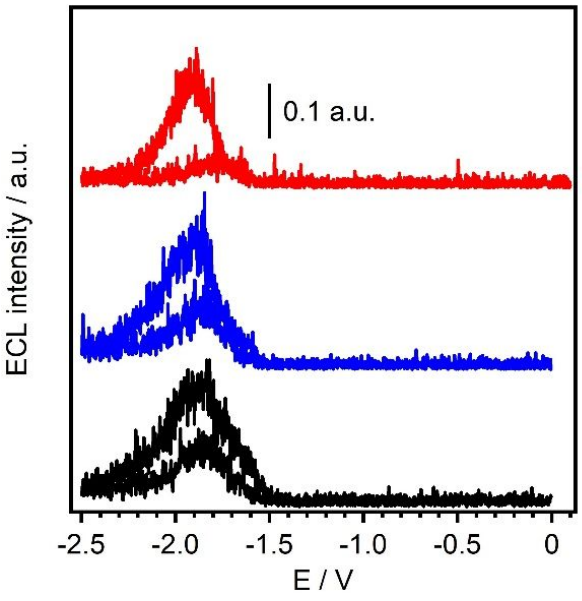

Figure 3. ECL emission for 10 µM $Ru(bpy)_3Cl_2$ with different coreactants (pH 7): 25 mM Na_2CO_3 (red) with potential first scanned to 2.5 V then −2.5 V; 10 mM H_2O_2 (blue) and 6.7 mM Na_2CO_3•$1.5H_2O_2$ (black) in 100 mM $NaClO_4$ with potential scanned from 0 V to −2.5 V. Scan rate was 100 mV/s. The signals have been shifted for clarity.

In order to support the hypothesis of the ECL mechanism with H_2O_2, we carried out experiments comparing carbonate solution with percarbonate (Na_2CO_3•$1.5H_2O_2$), and hydrogen peroxide solutions (Figure 3, Figure S5). The two solutions contained the same amount of hydrogen peroxide at a concentration of 10 mM and the CVs were directly swept from 0 V to −2.5 V. The ECL signals appear to be similar in all three systems, therefore supporting the hypothesis that hydrogen peroxide is the coreactant in the $Ru(bpy)_3^{2+}/CO_3^{2-}$ system, as outlined in the reaction sequence given in eqs 6-9.

Furthermore, the ECL emission was found to be quenched when DMSO, a well-known OH• scavenger,[50,51] was added to the solution (Figure S9). The residual ECL emission can be ascribed to the annihilation reaction (eq. 10). This highlights the role of OH• in the ECL mechanism.[52]

To gain an insight into the ECL emission mechanism of the present system, the effect of the oxidation potential was investigated using two-potential step chronoamperometry (CA). In the first step, an oxidation potential is applied for a fixed time (1s), while in the second step a potential of −2.0 V triggers the ECL reaction (Figure 4). The ECL signal in the second step was integrated to quantify the emission as a function of the oxidation potential of the first step (Figure 4, inset). The ECL emission was found to increase linearly from 1.8 V to 2.5 V, which indicates an increase in hydrogen peroxide from the electrogenerated peroxydicarbonate. The weak ECL emission at 1.5 V was assumed to be due to the annihilation reaction of $Ru(bpy)^{2+}$ (eq 10), similar to that obtained by cyclic voltammetry (Figure S8). The present ECL system can work at a potential of 1.8 V, which is 500 mV lower than that with our previously reported $Ru(bpy)_3^{2+}/SO_4^{2-}$ system (Figure S10, S11).

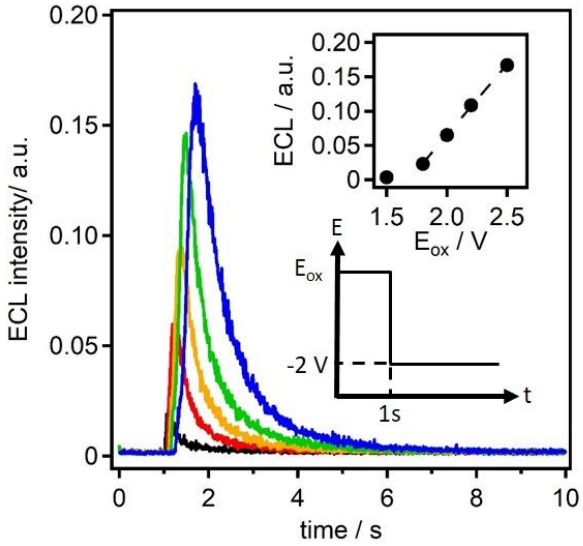

Figure 4. ECL intensity for 100 mM Na_2CO_3 and 10 µM $Ru(bpy)_3Cl_2$ by two-step chronoamperometry: $E_1 = E_{ox}$ V, t_{ox} = 1 s; E_2 = −2.0 V, t_2 = 9 s. Potentials: 1.5 V (black), 1.8 V (red), 2.0 V (orange), 2.2 V (green), and 2.5 V (blue). Insets: (top) plot of integrated ECL as a function of oxidation potential; (bottom) applied potential used in the chronoamperometry.

Furthermore, the influence of the oxidation time (t_{ox}) on the system was also investigated by CA to find the highest ECL emission. The current measured at a potential of 2.5 V during the first step in the presence of carbonate was integrated and found to increase linearly with the square root of oxidation time (Figure 5a), suggesting that the oxidation process was controlled by carbonate diffusion,[52] with increasing amounts of peroxydicarbonate, therefore hydrogen peroxide. On the other hand, the integrated ECL emission showed an increase up to 5 s, then nearly stable emission up to 20 s (Figure 5b). The ECL is highly affected by the gradient of the coreactant in the diffusion layer, which gives a lower peak intensity and broader emission. In fact, the diffusion layer thickness for carbonate with 1 to 20 s oxidation times ranges roughly from 100 to 600 µm.[53,54] This results in broader ECL emission and an increased delay time to reach the maximum intensity (Figure S12).

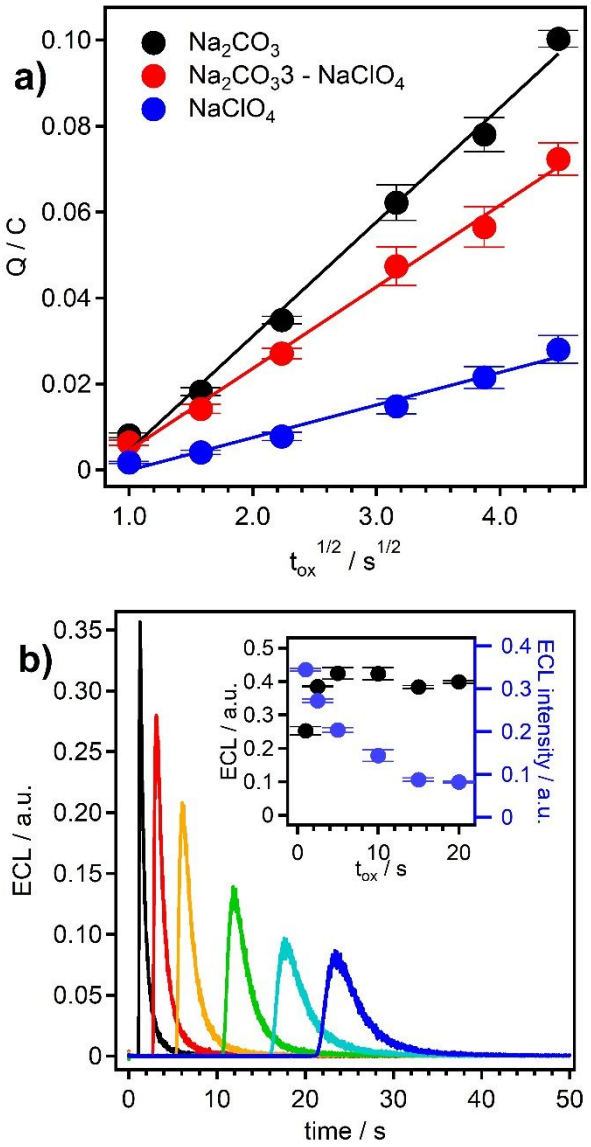

Figure 5. a) Integrated charge at 2.5 V for different oxidation times for 10 µM $Ru(bpy)_3Cl_2$ in 100 mM Na_2CO_3 (black), 100 mM $NaClO_4$ (blue), and the difference (red). b) ECL intensity by chronoamperometry: E_1 = 2.5 V, t_{ox} = 1s (black), 2.5s (red), 5s (orange), 10s (green), 15s (sky blue), and 20s (blue); E_2 = −2.0 V, t_2 = 30 s. Inset: plot of integrated ECL (black), and ECL intensity peak (blue) as a function of oxidation time.

The effect of pH on the ECL signal was investigated using CV measurements from pH 11.5, the pH of the starting Na_2CO_3 solution, to pH 4 (Figure 6). The oxidation current, ascribed to CO_3^{2-}, was found to decrease with decreasing pH (Figure S13), suggesting less peroxydicarbonate, and thus less H_2O_2, was generated. This might be the effect of pH on the equilibrium of the carbonate species, with the following reactions:

$$CO_3^{2-} + H_2O \rightleftharpoons HCO_3^- + OH^- \quad \text{pKa} = 10.33 \quad (11)$$

$$HCO_3^- + H_2O \rightleftharpoons H_2CO_3 + OH^- \quad \text{pKa} = 6.35 \quad (12)$$

$$H_2CO_3 \rightleftharpoons CO_{2(aq)} + H_2O \quad (13)$$

$$CO_{2(aq)} \rightleftharpoons CO_{2(g)} \quad (14)$$

In the neutral region, the concentration of carbonate is less dominant compared to the bicarbonate, and as the current decreases in the oxidation scan, we can infer that it is the carbonate ions that is oxidized rather than hydrogenated species such as bicarbonate or carbonic acid. However, the ECL signal increases as the pH decreases from 11.5, reaching a maximum at pH 7, while a further decrease down to pH 4 almost suppresses the ECL completely. In this case, the stability of the hydrogen peroxide generated in the solution seems to be the main factor for the ECL emission, since hydrogen peroxide is more stable when the pH is neutral or acidic.[55–57] Moreover, carbonate can promote the decomposition of hydrogen peroxide.[58] In conclusion, the ECL emission peak at pH 7 is due to two trends, (i.e., the decreasing CO_3^{2-} oxidation current and the increasing $OH^\bullet$ stability). Hydrogen evolution at pH 4 can hardly be the reason for the decrease in ECL, since we have already demonstrated that this pH does not affect the ECL emission at BDD electrode.[19]

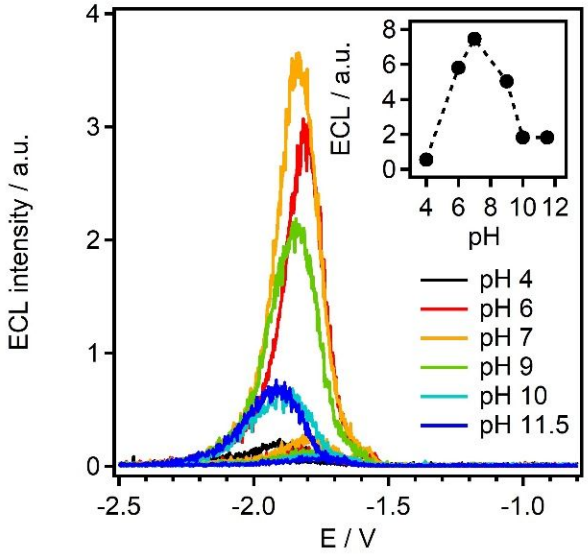

Figure 6. ECL intensity by cyclic voltammetry for 100 mM Na_2CO_3 and 10 µM $Ru(bpy)_3Cl_2$ with different pH adjusted by adding appropriate amounts of $HClO_4$ to the solution. The potential was first swept to 2.5 V then −2.5 V with a scan rate of 100 mV/s. Inset: plot of integrated ECL intensity as a function of pH.

The ECL emission as a function of Na_2CO_3 concentration was investigated from 25 mM to 1000 mM using CA (Figure 7). In the present system, the ECL signal is stable (Figure S14)

and it was found to be linear within the range of 25 mM to 200 mM (Figure S15) and reaches a plateau at 500 mM Na_2CO_3. The decrease at 1 M Na_2CO_3 can be explained by the possibility of hydrogen peroxide quenching the $Ru(bpy)_3^{2+}$*, since it can be seen that the carbonate oxidation charge (Figure S16) increased with carbonate concentration, suggesting that hydrogen peroxide is also increasing. This phenomena has previously been reported by Choi and Bard[18] with the maximum ECL emission achieved at 1 mM of H_2O_2 in 100 μM $Ru(bpy)_3Cl_2$ in a pH 7.5 phosphate buffer, with a quenching rate constant of 5.7×10^6 M^{-1} s^{-1}.

In our experimental setup, equivalent ECL emission was obtained in the linear range with a sensitivity to hydrogen peroxide of $0.015\times[H_2O_2]$/mM (Figure S17) compared to a sensitivity to carbonate of $0.003\times[CO_3^{2-}]$/mM (Figure 7, inset).

The ECL relative efficiency, compared to H_2O_2 is 20% and it reaches the maximum at 200 mM of CO_3^{2-} (Figure S16).

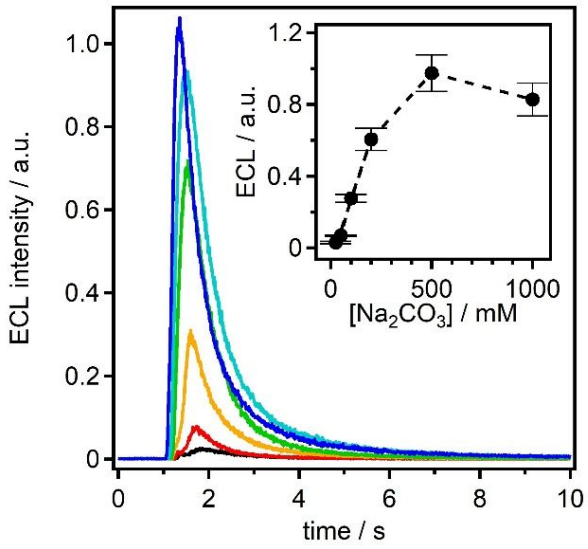

Figure 7. ECL intensity for 10 μM $Ru(bpy)_3Cl_2$ in 25 mM (black), 50 mM (red), 100 mM (orange), 200 mM (green), and 500 mM (sky blue), 1000 mM (blue) Na_2CO_3 solutions. Two-step chronoamperometry: $E_1 = 2.5$ V, $t_1 = 1$ s; $E_2 = -2$ V, $t_2 = 9$ s. Inset: integrated ECL as a function of Na_2CO_3 concentration.

Finally, we considered the energy needed to form $Ru(bpy)_3^{2+}$*. The Gibbs free energy for formation of the excited state, ΔG_{es}, can be written as:[59]

$$\Delta G_{es}\,(eV) \approx E^{0\prime}(Ru(bpy)^{2+/+}) - E^{0\prime}(OH^{\bullet}/OH^{-}) + E_{es}(Ru(bpy)_3^{2+*})$$

where E_{es} is the energy of the excited state of $Ru(bpy)_3^{2+}$* (2.12 eV).[18] $E^{0\prime}(Ru(bpy)^{2+/+}$ is −1.28 V (vs SHE), while $E^{0\prime}(OH^{\bullet}/OH^{-})$ is 1.77 - 1.91 V (vs SHE)[27-29], therefore the ΔG_{es} is −0.93/1.07 eV, enough to populate the excited states of $Ru(bpy)_3^{2+}$.

Further, the contribution of peroxydicarbonate cannot be overlooked, since it is present in the diffusion layer and may act as a coreactant. In fact, the redox potential of the couple $CO_3^{\bullet-}/CO_3^{2-}$ is similar to that of the hydroxyl radical, $E^{0\prime} = 1.59$ V,[33-35] enough to excite the $Ru(bpy)_3^{2+}$. This may explain the residual ECL signal when DMSO is used to quench the $OH^{\bullet}$, in addition to annihilation reaction.

The contributions of carbonate oxidation and hydrogen peroxide in the present ECL system were investigated by ATR-IR spectroscopy, as we previously demonstrated for other electrochemical systems.[60–63]

In the first instance, we recorded the spectra of carbonate and hydrogen peroxide which are the main species involved in the ECL reaction, in order to identify the two features of interest, where both compounds have an absorption at ≈ 1370 - 1380 cm^{-1} (Figure S18). The oxidation of carbonate gave a negative peak (Figure S19) as a result of depletion near the electrode surface; however, this intensity decreased, and an almost identical wavenumber prevented direct identification of hydrogen peroxide. A clear difference in absorption intensity for carbonate oxidation was observed if performed in H_2O or D_2O, therefore we inferred a different reactivity for peroxydicarbonate hydrolysis.[64] Spectra collected in the potential region of ECL emission showed an intense peak at 1380 cm^{-1} only for carbonate in H_2O, while carbonate in D_2O and perchlorate in H_2O (i.e., BG) did not show this signal (Figure 8, S20).

We ascribe this absence of a peak at 1380 cm^{-1} to slow or even no peroxydicarbonate hydrolysis to generate hydrogen peroxide in D_2O. This also implies that $OH^{\bullet}$ is not a source of hydrogen peroxide in this electrochemical system (Figure 8, black line), which agrees with lack of relevant ECL emission in $NaClO_4$. Interestingly, this IR peak starts at a potential of −1.5 V (Figure S21), the same potential at which the ECL signal appears (Figure 2, red line), and has a lower intensity in the presence of $Ru(bpy)_3^{2+}$ (Figure S22) as hydrogen peroxide is consumed in the ECL reaction.

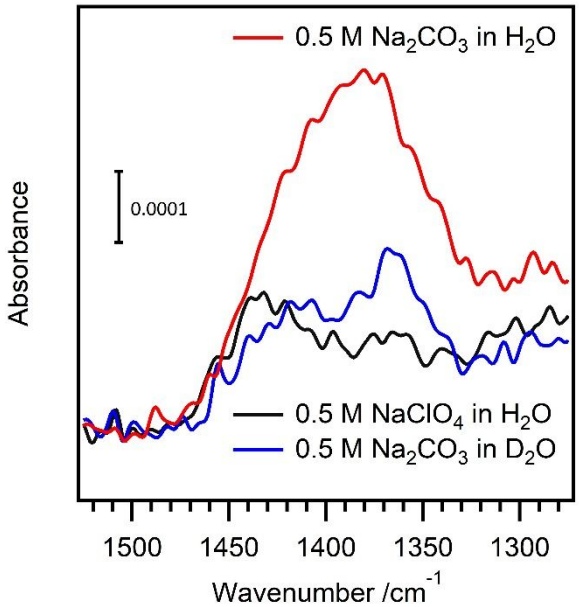

Figure 8. ATR-IR spectra on a BDD electrode in 0.5 M Na_2CO_3 in H_2O (red) and in D_2O (blue), and 0.5 M $NaClO_4$ in H_2O (black). Each spectrum was measured at $E_{base} = -2.5$ V after 20 seconds oxidation pulse at 2.5 V.

CONCLUSION

A coreactant-free ECL system using $Ru(bpy)_3^{2+}$ as the luminophore in aqueous solutions containing carbonate is reported. The underlying mechanism involves the oxidation of

carbonate to peroxydicarbonate, which hydrolysis leads to the in-situ production of the coreactant, hydrogen peroxide. This ECL system was made possible only by using a BDD electrode, which has a wide potential window and promotes direct oxidation of hydroxide, allowing the mediated oxidation of carbonate, while at the same time suppressing hydrogen evolution at the cathodic currents where the ECL reaction takes place. The ECL emission was found to be dependent on the carbonate concentration, so can be applied to carbonate detection, while it can be controlled by several parameters such as the pH, the oxidation potential and time to tune the ECL intensity.

ASSOCIATED CONTENT

Supporting Information

Raman spectra and SEM image of BDD, ATR-IR and ATR-SNIFTIRS set-up, ECL at BDD, GC and Pt electrodes, comparison of counteranion (chlorine and perchlorate), effect of nitrogen bubbling after oxidation on the reduction current, current of $Ru(bpy)_3Cl_2$ with different coreactants, ECL spectra, ECL without $Ru(bpy)_3^{2+}$, ECL at different scanned potentials, influence of DMSO on the ECL emission, comparison between carbonate and sulfate solutions at different potentials, integrated ECL for carbonate and sulfate solutions as a function of oxidation potential, ECL delay time, CV current signal at different pH, inter and intra-electrode reproducibility, integrated ECL as a function of Na_2CO_3 concentration, integrated anodic charge as a function of Na_2CO_3 and relative ECL efficiency, ECL emission as a function of H_2O_2 concentration, ATR-IR spectra for Na_2CO_3 and H_2O_2, ATR-SNIFTIRS for Na_2CO_3 in H_2O and in D_2O, time dependent oxidation ATR-IR spectra for Na_2CO_3 in H_2O, ATR-IR spectra for Na_2CO_3 in H_2O and in D_2O at different E_{base}, ATR-IR spectrum for $Ru(bpy)_3Cl_2$ and Na_2CO_3 in H_2O,.

AUTHOR INFORMATION

Corresponding Author

* Y.E. einaga@chem.keio.ac.jp;

ORCID

Irkham: 0000-0001-9938-2931

Andrea Fiorani: 0000-0001-8413-6439

Giovanni Valenti: 0000-0002-6223-2072

Francesco Paolucci: 0000-0003-4614-8740

Yasuaki Einaga: 0000-0001-7057-4358

ACKNOWLEDGMENT

I. acknowledges a “Design the Future” International Student Award, Keio University.

A. F. acknowledges the Japan Society for the Promotion of Science (fellowship ID No. P19333) and Grant-in-Aid for JSPS Fellows (19F19333).

REFERENCES

(1) Ronkainen, N. J.; Halsall, H. B.; Heineman, W.R. Electrochemical biosensors. *Chem. Soc. Rev.* **2010**, *39*, 1747-1763.

(2) Wang, Z.; Yu, R.; Zeng, H.; Wang, X.; Luo, S.; Li, W.; Luo, X.; Yang, T. Nucleic acid-based ratiometric electrochemiluminescent, electrochemical and photoelectrochemical biosensors: a review. *Microchim. Acta.* **2019**, *186*, 1-19.

(3) Zanut, A.; Fiorani, A.; Rebeccani, S.; Kesarkar, S.; Valenti, G. Electrochemiluminescence as emerging microscopy techniques. *Anal. Bional. Chem.* **2019**, *411*, 4375-4382.

(4) Gao, W.; Saqib, M.; Qi, L.; Zhang, W.; Xu, G. Recent advances in electrochemiluminescence devices for point-of-care testing. *Curr. Opin. Electrochem.* **2017**, *3*, 4-10.

(5) Miao, W. Electrogenerated Chemiluminescence and Its Biorelated Applications. *Chem. Rev.* **2008**, *108*, 2506-2553.

(6) Richter, M. M. Electrochemiluminescence (ECL). *Chem. Rev.* **2004**, *104*, 3003-3036.

(7) Hesari, M.; Ding, Z. Review-Electrogenerated Chemiluminescence: Light Years Ahead. *J. Electrochem. Soc.* **2016**, *163*, 3116-3131.

(8) Fiorani, A.; Valenti, G.; Iurlo, M.; Marcaccio, M.; Paolucci, F. Electrogenerated chemiluminescence: A molecular electrochemistry point of view. *Curr. Opin. Electrochem.* **2018**, *8*, 31-38.

(9) Leland, J. K.; Powell, M. J. Electrogenerated Chemiluminescence: An Oxidative-Reduction Type ECL reaction sequence using tripropyl amine. *J. Electrochem. Soc.* **1990,** *137*, 3127–3131.

(10) White, H. S.; Bard, A. J. Electrogenerated chemiluminescence. 41. Electrogenerated chemiluminescence and chemiluminescence of the $Ru(2,2'\text{-}bpy)_3^{2+}$-$S_2O_8^{2-}$ system in acetonitrile-water solutions. *J. Am. Chem. Soc.* **1982**, *104*, 6891-6895.

(11) Muzyka, K. Current trends in the development of the electrochemiluminescent immunosensors. *Biosens. Bioelectron.* **2014**, *54*, 393-407.

(12) Liu, Z.; Qi, W.; Xu, G. Recent advances in electrochemiluminescence. *Chem. Soc. Rev.* **2015**, *44*, 3117-3142.

(13) Valenti, G.; Fiorani, A.; Li, H.; Sojic, N.; Paolucci, F. Essential role of electrode materials in electrochemiluminescence applications. *ChemElectroChem* **2016**, *3*, 1990-1997.

(14) Zu, Y.; Bard, A. J. Electrogenerated chemiluminescence. 66. The role of direct coreactant oxidation in the ruthenium tris(2,2’)bipyridyl/tripropylamine system and the effect of halide ions on the emission intensity. *Anal. Chem.* **2000**, *72*, 3223-3232.

(15) Chen, Z.; Zu, Y. Electrogenerated chemiluminescence of the tris(2,2′-bipyridine) ruthenium(II)/tri-n-propylamine (TPrA) system: Crucial role of the long lifetime of $TPrA^+$ cation radicals suggested by electrode surface effects. *J. Phys. Chem. C* **2008**, *112*, 16663-16667.

(16) Villani, E.; Valenti, G.; Marcaccio, M.; Mattarozzi, L.; Barison, S.; Garoli, D.; Cattarin, S.; Paolucci, F. Coreactant electrochemiluminescence at nanoporous gold electrodes. *Electrochim. Acta* **2018**, *277*, 168-175.

(17) Xu, G.; Dong, S. Electrochemiluminescence of the $Ru(bpy)_3^{2+}$/ $S_2O_8^{2-}$ system in purely aqueous solution at carbon paste electrode. *Electroanalysis* **2000**, *12*, 583-587.

(18) Choi, J. P.; Bard, A. J. Electrogenerated chemiluminescence (ECL) 79. Reductive-oxidation ECL of tris(2,2′-bipyridine) ruthenium(II) using hydrogen peroxide as a coreactant in pH 7.5 phosphate buffer solution. *Anal. Chim. Acta* **2005**, *541*, 143-150.

(19) Fiorani, A.; Irkham; Valenti, G.; Paolucci, F.; Einaga, Y. Electrogenerated chemiluminescence with peroxydisulfate as a coreactant using boron doped diamond electrodes. *Anal. Chem.* **2018**, *90*, 15636-15641.

(20) Irkham; Watanabe, T.; Fiorani, A.; Valenti, G.; Paolucci, F.; Einaga, Y. Co-reactant-on-Demand ECL: Electrogenerated chemiluminescence by the in Situ production of $S_2O_8^{2-}$ at boron-doped diamond electrodes. *J. Am. Chem. Soc.* **2016**, *138*, 15636-15641.

(21) Memming, R. Mechanism of the electrochemical reduction of persulfates and hydrogen peroxide. *J. Electrochem. Soc.* **1969**, *116*, 785-790.

(22) Eberson, L. Electron-transfer reactions in organic chemistry. *Adv. Phys. Org. Chem.* **1982**, *18*, 79-185.

(23) Michaud, P. A.; Mahé, E.; Haenni, W.; Perret, A.; Comninellis, C. Preparation of peroxodisulfuric acid using boron-doped diamond thin film electrodes. *Electrochem. Solid-State Lett.* **2000**, *3*, 77-79.

(24) Marselli, B.; Garcia-Gomez, J.; Michaud, P.-A.; Rodrigo, M. A.; Comninellis, C. Electrogeneration of hydroxyl radicals on boron-doped diamond electrodes. *J. Electrochem. Soc.* **2003**, *150*, 79-83.

(25) Thostenson, J. O.; Ngaboyamahina, E.; Sellgren, K. L.; Hawkins, B. T.; Piascik, J. R.; Klem, E. J. D.; Parker, C. B.; Deshusses, M. A.; Stoner, B. R.; Glass, J. T. Enhanced H_2O_2 Production at reductive potentials from oxidized boron-doped ultrananocrystalline diamond electrodes. *ACS Appl. Mater. Interfaces* **2017**, *9*, 16610-16619.

(26) Katsuki, N. Water electrolysis using diamond thin-film electrodes. *J. Electrochem. Soc.* **1998**, *145*, 2358-2362.

(27) Koppenol, W. H.; Liebman, J. F. The oxidizing nature of the hydroxyl radical. A comparison with the ferryl ion (FeO^{2+}). *J. Phys. Chem.* **1984**, *88*, 99-101.

(28) Schwarz, H. A.; Dodson, R. W. Equilibrium between hydroxyl radicals and thallium(II) and the oxidation potential of OH(aq). *J. Phys. Chem.* **1984**, *88*, 3643-3647.

(29) Kläning, U. K.; Sehested, K.; Holcman, J. Standard Gibbs energy of formation of the hydroxyl radical in aqueous solution. Rate constants for the reaction $ClO_2^- + O_3 \rightleftarrows O_3^- + ClO_2$. *J. Phys. Chem.* **1985**, *89*, 760-763.

(30) Leca, B.; Blum, L. J. Luminol electrochemiluminescence with screen-printed electrodes for low-cost disposable oxidase-based optical sensors. *Analyst* **2000**, *125*, 789-91.

(31) Sakura, S. Electrochemiluminescence of hydrogen peroxide-luminol at a carbon electrode. *Anal. Chim. Acta* **1992**, *262*, 49-57.

(32) Martin, H. B. Hydrogen and oxygen evolution on boron-doped diamond electrodes. *J. Electrochem. Soc.* **1996**, *143*, 133-136.

(33) Zuo, Z.; Cai, Z.; Katsumura, Y.; Chitose, N.; Muroya, Y. Reinvestigation of the acid-base equilibrium of the (bi)carbonate radical and ph dependence of its reactivity with inorganic reactants. *Radiat. Phys. Chem.* **1999**, *55*, 15-23.

(34) Bisby, R. H.; Johnson, S. A.; Parker, A. W.; Tavender, S. M. Time-resolved resonance raman spectroscopy of the carbonate radical. *J. Chem. Soc. Faraday Trans.* **1998**, *94*, 2069-2072.

(35) Huie, R. E.; Clifton, C. L.; Neta, P. Electron transfer reaction rates and equilibria of the carbonate and sulfate radical anions. *Radiat. Phys. Chem.* **1991**, *38*, 477-481.

(36) Ruiz, E. J.; Ortega-Borges, R.; Jurado, J. L.; Chapman, T. W.; Meas, Y. Simultaneous anodic and cathodic production of sodium percarbonate in aqueous solution. *Electrochem. Solid-State Lett.* **2009**, *12*, 1-4.

(37) Saha, M. S.; Furuta, T.; Nishiki, Y. Conversion of carbon dioxide to peroxycarbonate at boron-doped diamond electrode. *Electrochem. Commun.* **2004**, *6*, 201-204.

(38) Velazquez-Peña, S., Sáez, C.; Cañizares, P.; Linares-Hernández, I.; Martínez-Miranda, V.; Barrera-Díaz, C.; Rodrigo, M. A. Production of oxidants via electrolysis of carbonate solutions with conductive-diamond anodes. *Chem. Eng. J.* **2013**, *230*, 272-278.

(39) Saha, M. S.; Furuta, T.; Nishiki, Y. Electrochemical synthesis of sodium peroxycarbonate at boron-doped diamond electrodes. *Electrochem. Solid-State Lett.* **2003**, *6*, 5-7.

(40) Zhang, J.; Oloman, C. W. Electro-oxidation of carbonate in aqueous solution on a platinum rotating ring disk electrode. *J. Appl. Electrochem.* **2005**, *35*, 945-953.

(41). Flanagan, J.; Jones, D. P.; Griffith, W. P.; Skapski, A. C.; West, A. P. On the existence of peroxocarbonates in aqueous solution. *J. Chem. Soc. Commun.* **1986**, *1*, 20-21.

(42) Michaud, P-A.; Panizza, M.; Outtara, L.; Diaco, T.; Foti, G.; Comninellis, C. Electrochemical oxidation of water on synthetic boron-doped diamond thin film anodes. *J. Appl. Electrochem.* **2003**, *33*, 151-154.

(43) Macpherson, J. V. A practical guide to using boron doped diamond in electrochemical research. *Phys. Chem. Chem. Phys.* **2015**, *17*, 2935-2949.

(44) Irkham; Watanabe, T.; Einaga, Y. Hydroxide ion oxidation in aqueous solutions using boron-doped diamond electrodes. *Anal. chem.* **2017**, *89*, 7139-7144.

(45) Irkham; Einaga, Y. Oxidation of hydroxide ions in weak basic solutions using boron-doped diamond electrodes: effect of the buffer capacity. *Analyst* **2019**, *144*, 4499-4504.

(46) Mahé, É.; Bornoz, P.; Briot, E.; Chevalet, J.; Comninellis, C.; Deviliers, D. A selective chemiluminescence detection method for reactive oxygen species involved in oxygen reduction reaction on electrocatalytic materials. *Electrochim. Acta* **2013**, *102*, 259-273.

(47) Watanabe, T.; Honda, Y.; Kanda, K.; Einaga, Y. Tailored design of boron-doped diamond electrodes for various electrochemical applications with boron-doping level and sp2-bonded carbon impurities. *Phys. Status Solidi A* **2014**, *211*, 2709-2717.

(48) Kapałka, A.; Fóti, G.; Comninellis, C. The importance of electrode material in environmental electrochemistry. Formation and reactivity of free hydroxyl radicals on boron-doped diamond electrodes. *Electrochim. Acta* **2009**, ***254***, 2018-2023.

(49) Tokel, N. E.; Bard, A. J. Electrogenerated Chemiluminescence. IX. Electrochemistry and emission from systems containing tris(2,2′-bipyridine)ruthenium(II) dichloride. *J. Am. Chem. Soc.* **1972**, *94*, 2862-2863.

(50) Garcia-Segura, S.; Centellas, F.; Brillas, E. Unprecedented electrochemiluminescence of luminol on a boron-doped diamond thin-film anode. Enhancement by electrogenerated superoxide radical anion. *J. Phys. Chem. C* **2012**, *116*, 15500-15504.

(51) Bardouki, H.; Barcellos da Rosa, M.; Mihalopoulos, N.; Palm, W.-U.; Zetzsch, C. Kinetics and mechanism of the oxidation of dimethylsulfoxide (DMSO) and methanesulfinate (MSI^-) by OH radicals in aqueous medium. *Atmospheric Environ.* **2002**, *36*, 4627-4634.

(52) Bard, A. J.; Faulkner, L. R. *Electrochemical Methods. Fundamentals and Applications, 2nd Edition;* John Wiley & Sons, Inc.: New York, **2001**; pp 210-216.

(53) Bard, A. J.; Faulkner, L. R. *Electrochemical Methods. Fundamentals and applications, 2nd Edition;* John Wiley & Sons, Inc.: New York, **2001**; pp 34-35.

(54) Zeebe, R. E. On the molecular diffusion coefficients of dissolved CO_2, HCO_3^-, and CO_3^{2-} and their dependence on isotopic mass. *Geochim. Cosmochim. Acta* **2011**, *75*, 2483-2498.

(55) Duke, F. R.; Haas, T. W. The homogeneous base-catalyzed decomposition of hydrogen peroxide. *J. Phys. Chem.* **1961**, *65*, 304-306.

(56) Staehelin, J.; Holgné, J. Decomposition of ozone in water: Rate of initiation by hydroxide ions and hydrogen peroxide. *Environ. Sci. Technol.* **1982**, *16*, 676-681.

(57) Hickel, B.; Corfitzen, H.; Sehested, K. Measurement of the rate constants of the reactions $OH + OH^- \rightleftarrows O^- + H_2O$ and $OD + OD^- \rightleftarrows O^- + D_2O$ in forward and reverse directions. Kinetic determination of the pK's of OH and OD radicals. *J. Phys. Chem.* **1996**, *100*, 17186-17190.

(58) Lee, H. H. B.; Park, A. H.; Oloman, C. W. Stability of hydrogen peroxide in sodium carbonate solutions. *TAPPI J.* **2000**, *83*, 94-102.

(59) Valenti, G.; Rampazzo, E.; Kesarkar, S.; Genovese, D.; Fiorani, A.; Zanut, A.; Palomba, F.; Marcaccio, M.; Paolucci, F.; Prodi, L.

Electrogenerated chemiluminescence from metal complexes-based nanoparticles for highly sensitive sensors applications. *Coord. Chem. Rev.* **2018**, *367*, 65-81.

(60) Ogose, T., Kasahara, S., Ikemiya, N., Hoshi, N., Einaga, Y.,Nakamura, M. In Situ ATR-IR Observation of the Electrochemical Oxidation of a Polycrystalline Boron-Doped Diamond Electrode in Acidic Solutions. *J. Phys. Chem.* **2018**, *122*, 27456-27461.

(61) Tomisaki, M., Kasahara, S., Natsui, K., Ikemiya, N. & Einaga, Y. Switchable product selectivity in the electrochemical reduction of carbon dioxide using boron-doped diamond electrodes. *J. Am. Chem. Soc* **2019**, *141*, 7414-7420.

(62) Kasahara, S., Ogose, T., Ikemiya, N., Yamamoto, T., Natsui, K., Yokota, Y., Wong, R. A., Izuka, S., Hoshi, N., Tateyama, Y., Kim, Y., Nakamura, M., Einaga, Y. In Situ spectroscopic study on the surface hydroxylation of diamond electrodes. *Anal. Chem.* **2019**, *91*, 4980-4986.

(63) Kamoshida, N.; Kasahara, S.; Ikemiya, N.; Hoshi, N.; Nakamura, M.; Einaga, Y. In situ ATR-IR study of $Fe(CN)_6^{3-}$ /$Fe(CN)_6^{4-}$ redox system on boron-doped diamond electrode. *Diamond Relat. Mater.* **2019**, *93*, 50-53.

(64) Wiberg, K. B. The deuterium isotope effect. *Chem. Rev.* **1955**, *55*, 713-743.

Table of Content